Supplementary Information for

How Low-Temperature Welding Affects the Nanostructure of Nanowire Junctions

Matteo Ferliga   Davide Grazioli   Angelo Simone   Lucia Nicola

Department of Industrial Engineering, University of Padua, Italy
emails: {matteo.ferliga, davide.grazioli, angelo.simone, lucia.nicola}@unipd.it

1 Interpenetration factor definition and convergence criterion

To quantify the interpenetration between nanowires (NWs), we define the interpenetration factor

$$IF = \frac{\mathrm{h}_0^z - \mathrm{h}_\mathrm{f}^z}{\mathrm{h}_0^z}, \tag{1}$$

where h^z denotes the vertical component of the distance between the centers of mass of the NWs. The coordinate vector $\boldsymbol{\chi}^i$ of the center of mass of the i-th NW is computed as

$$\boldsymbol{\chi}^i = \frac{1}{M^i} \sum_{j=1}^{n^i} m_j^i \boldsymbol{r}_j^i, \tag{2}$$

where m_j^i and $\boldsymbol{r}_j^i$ denote, respectively, the mass and position vector of the j-th atom, while $M^i = \sum_{j=1}^{n^i} m_j^i$ represents the sum of the masses of the atoms of the i-th NW. The scalar quantity h^z is therefore defined as the absolute value of the projection of $\boldsymbol{\chi}^2 - \boldsymbol{\chi}^1$ onto the z axis in Figure S1. In definition (1), h_0^z indicates the initial center-of-mass separation at the onset of heating, while h_f^z denotes its vertical component at a given time step. We compute IF (1) at each time increment of the numerical simulation. The limiting cases of no interpenetration and complete interpenetration correspond to $IF = 0$ and $IF = 1$, respectively. The localized welding protocol imposes a temperature gradient along the longitudinal axis of the NWs, with a hot junction region and cold ends, which may induce bending. Bending primarily occurs during the initial stages of the process and subsides once equilibrium is established. To accurately capture interpenetration throughout the welding process, we compute the center of mass of each NW by considering only the atoms belonging to the heated region. Accordingly, the term n^i in Eq. (2) represents the number of yellow-shaded atoms in Figure S1 that belong to the i-th NW.

In our numerical simulations, the holding stage is nominally terminated once convergence of IF is achieved. In some cases, the holding duration was extended beyond the strict convergence time, or manually limited at high target temperature, in order to ensure consistency across simulations or to prevent morphological instabilities, as detailed in the main manuscript. We assess convergence by dividing the holding stage into intervals of 5×10^5 time steps (7.5 ns each) and computing the average IF value within each interval. Convergence is achieved when the absolute difference between

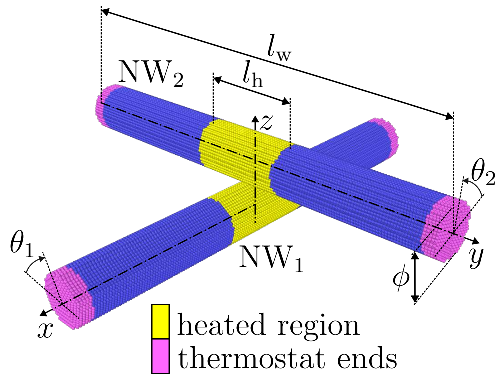

Figure S1: NW pair in a perpendicular arrangement. The yellow region denotes the atoms subject to heating, whereas the purple regions indicate the atoms kept at room temperature. Simulations are conducted for various values of the angles θ_1 and θ_2, as well as different target temperatures.

consecutive interval averages falls below 10^{-3}, at which point the simulation proceeds to the cooling stage. In some cases, the holding time was adjusted for consistency across target temperatures, as detailed in the main manuscript.

2 Nanowire and junction assembly

Penta-twinned NW structures are generated by joining five prisms with isosceles triangular bases and a vertex angle of 70.53°. This procedure leads to the formation of the {111} twin planes and a 7.35° angular gap as illustrated in Figure S2(a). As pointed out by De Wit [2], the gap closure can be described as a positive partial wedge disclination with its Frank vector aligned with the nanowire centerline. The extent of the angular gap that characterizes our structures is consistent with experimental observations. Gao et al. [3], for example, performed high-resolution transmission electron microscopy (HRTEM) on AgNWs synthesized via PVP-assisted (polyvinylpyrrolidone, PVP-K30) polyol reduction and identified an angular gap of 7.5°. As a result of the closure of the gap, the NW is internally strained in its relaxed state [6] and is therefore characterized by a self-equilibrated, non-uniform stress field [1, 4, 5, 7]. This behavior is also observed in our model after energy minimization at 0 K. The axial component of the stress tensor, σ_{zz}, is shown in Figure S2(b), indicating tensile stress at the surface and compressive stress in the interior of the cross-section. The stress range is significant, with values reaching the gigapascal scale. The results of the molecular dynamics simulations performed by Niekiel et al. [5] on PT AgNWs with a pentagonal cross-section present analogous stress patterns and values, therefore providing a qualitative validation of the structure preparation strategy. SC NW structures are generated using a procedure analogous to the one described above. However, unlike PT nanowires, SC nanowires do not experience internal stresses, apart from those induced by surface tension.

Junctions are created by arranging pairs of nanowires such that their axes are perpendicular but not coplanar, as illustrated in Figure S1. Before applying the welding thermal cycle described in the main manuscript, the assembled NW pair is brought from 0 K to room temperature over 80 ps and then relaxed at room temperature for 30 ps, with both steps performed in the NPT ensemble.

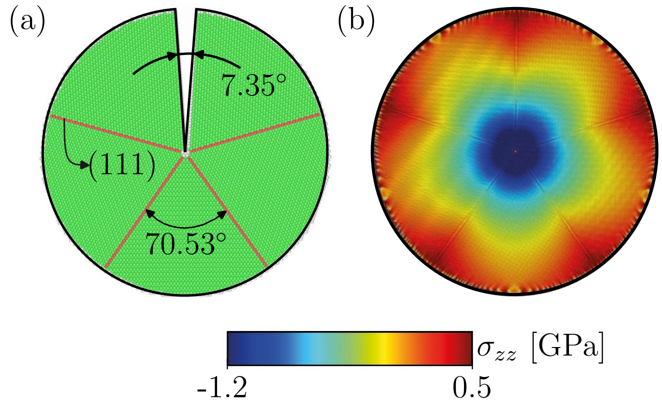

Figure S2: (a) Schematic illustration of the construction of a penta-twinned nanowire. The five face-centered cubic sectors are generated at an angle of 70.53° each, leaving an angular gap of 7.35°. Upon equilibration at 0 K, intrinsic stresses build up (b). The contour plot represents the stress field in the axial direction (σ_{zz}). Green atoms represent an FCC configuration, red atoms indicate an HCP configuration.

3 Supplementary figures

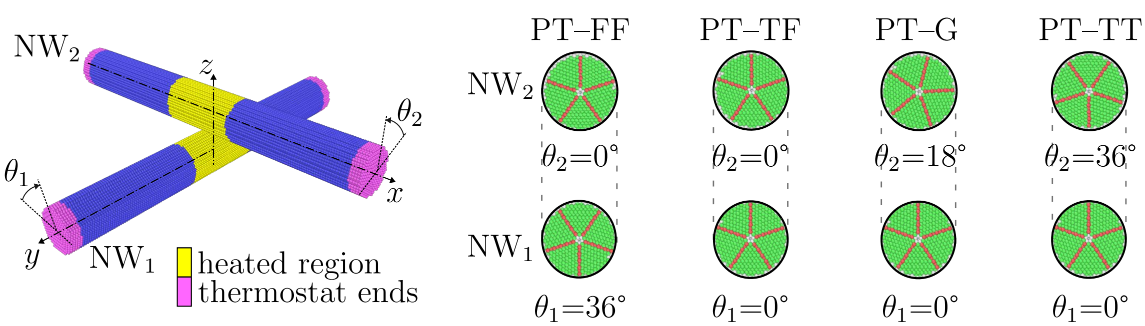

Figure S3: Owing to the fivefold symmetry of PT nanowires, the set of representative junction configurations reduces to three distinct configurations: PT–FF (face-to-face), PT–TF (twin-to-face), and PT–TT (twin-to-twin). For completeness, the generic configuration PT–G is also reported, corresponding to a relative rotation of 18° from PT–FF, and is used as a representative generic misorientation.

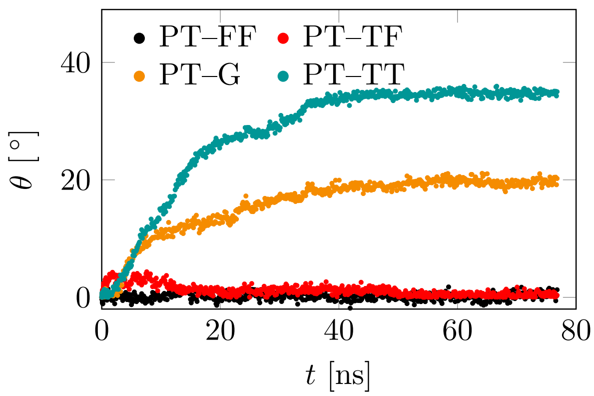

Figure S4: Rigid rotation of the top PT nanowire during welding at 0.6 T_{m} for PT–FF, PT–TF, PT–G, and PT–TT.

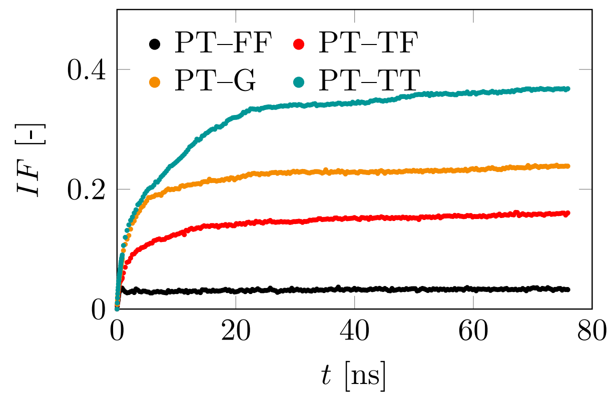

Figure S5: Interpenetration kinetics $IF(t)$ at 0.6 T_{m} for the four PT junction configurations. The curves increase during the heating and holding stages and then plateau, indicating convergence within 75.9 ns.

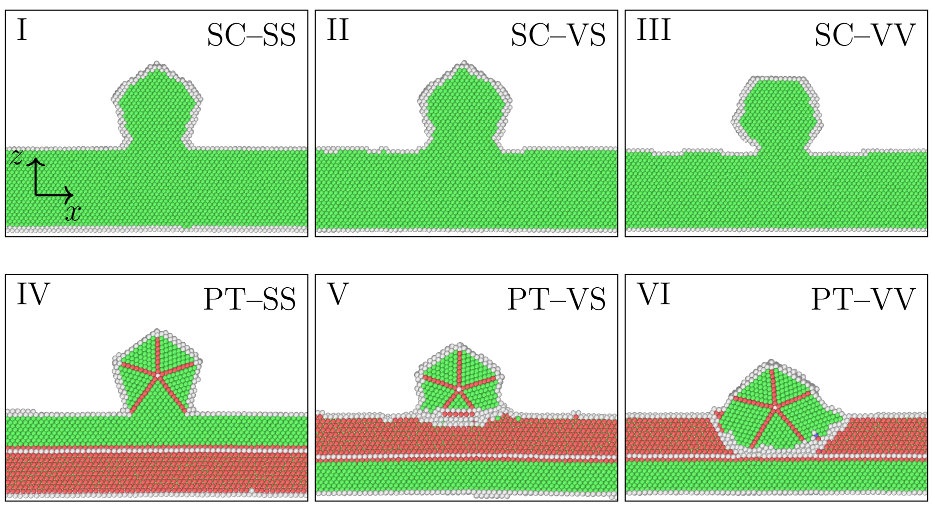

Figure S6: Effect of the relative orientation of the crystalline structure of NWs on the resulting junction. Cross-sectional views at the center of the junction by the yz plane. The panels show the nanostructure of the junction at the end of the post-welding stage.

References

[1] E. Bitzek, P. Koskinen, F. Gähler, M. Moseler, and P. Gumbsch. Structural relaxation made simple. *Physical Review Letters*, 97(17):170201, 2006.

[2] R. De Wit. Partial disclinations. *Journal of Physics C: Solid State Physics*, 5(5):529, 1972.

[3] Y. Gao, L. Song, P. Jiang, L. Liu, X. Yan, Z. Zhou, D. Liu, J. Wang, H. Yuan, Z. Zhang, X. Zhao, X. Dou, W. Zhou, G. Wang, S. Xie, H. Chen, and J. Li. Silver nanowires with five-fold symmetric cross-section. *Journal of Crystal Growth*, 276(3-4):606–612, 2005.

[4] J. Guénolé, W. G. Nöhring, A. Vaid, F. Houllé, Z. Xie, A. Prakash, and E. Bitzek. Assessment and optimization of the fast inertial relaxation engine (fire) for energy minimization in atomistic simulations and its implementation in LAMMPS. *Computational Materials Science*, 175:109584, 2020.

[5] F. Niekiel, E. Spiecker, and E. Bitzek. Influence of anisotropic elasticity on the mechanical properties of fivefold twinned nanowires. *Journal of the Mechanics and Physics of Solids*, 84:358–379, 2015.

[6] V. V. Radmilović, M. Göbelt, C. Ophus, S. Christiansen, E. Spiecker, and V. R. Radmilović. Low temperature solid-state wetting and formation of nanowelds in silver nanowires. *Nanotechnology*, 28(38):385701, 2017.

[7] D. Sheppard, R. Terrell, and G. Henkelman. Optimization methods for finding minimum energy paths. *The Journal of Chemical Physics*, 128(13), 2008.